APL Materials ARTICLE scitation.org/journal/apm

Automatic design of chiral mechanical metamaterials

Cite as: APL Mater. 9, 101112 (2021); doi: 10.1063/5.0066210
Submitted: 9 August 2021 • Accepted: 24 September 2021 •
Published Online: 12 October 2021

Lorenzo Beretta,[1] Silvia Bonfanti,[1,2] Jacopo Fiocchi,[3] Francesc Font-Clos,[1] Roberto Guerra,[1] Ausonio Tuissi,[3] and Stefano Zapperi[1,2,a)]

AFFILIATIONS

[1] Center for Complexity and Biosystems, Department of Physics, University of Milan, via Celoria 16, 20133 Milano, Italy
[2] CNR–Consiglio Nazionale delle Ricerche, Istituto di Chimica della Materia Condensata e di Tecnologie per l'Energia, Via R. Cozzi 53, 20125 Milano, Italy
[3] CNR–Consiglio Nazionale delle Ricerche, Istituto di Chimica della Materia Condensata e di Tecnologie per l'Energia, Via Previati 1/e, 23900 Lecco, Italy

[a)] **Author to whom correspondence should be addressed:** stefano.zapperi@unimi.it

ABSTRACT

Automatic design of mechanical metamaterials is key to achieving efficiencies in terms of a desired functionality that can far exceed the rationally designed man-made solutions. Here, we introduce a discrete element model capable of describing the mechanical response of three-dimensional trussed structures under a predetermined external perturbation and coupling it to an optimization algorithm in order to produce chiral mechanical metamaterials, twisting under compression and thus converting linear motion into rotation. By comparing the machine-designed structures with pre-existing human-designed solutions, we show that the former can achieve a much higher efficiency in terms of rotating angle per unit compressive strain. We confirm our results by finite element calculations and by experiments on 3D printed structures. The presented method paves the way to the discovery of novel functional mechanisms that can act over a broad size range, from micro- to macroscales, giving rise to a countless number of possible solutions for functional mechanical metamaterials.

I. INTRODUCTION

The design of materials with tailored mechanical properties and functionalities represents a major scientific and technological challenge with enormous potential for engineering and societal applications. Mechanical metamaterials, a recent class of artificial materials characterized by distinctive internal architecture, represent an interesting strategy to fulfill this need. Thanks to the careful assembly of cells or meshes, the structure is capable of producing exceptional properties and responses, rare or impossible to find in ordinary materials,[1] such as negative Poisson's ratio, negative compressibility, or elasticity. Countless ways to order and arrange sub-units in different architectures give rise to a vast variety of possibilities to design metamaterials with different properties,[2] with possible applications in many different fields.

Functional metamaterials or *metamaterial machines*,[3] which can perform mechanical functions by transforming input stimuli and movements into programmable outputs, represent a promising field of research with enormous potential for the industrial sector, given the drastic reduction in assembly complexity and the potential scalability of the process down to micron scale dimensions. Recent advances in additive manufacturing (3D printing) have made mass production and industrialization of the manufacture of complex and innovative design objects made in computer models technologically and economically feasible. This type of structures can have very interesting applications in all areas where a movement mode conversion is necessary, especially at very small scales where traditional actuators are not usable. Thanks to the advancement of miniaturization techniques, which allow us to print structures at the micron scale, this type of application will be increasingly accessible. Similar structures can then be combined into more complex mechanisms.

Metamaterial design is currently mostly based on a mix of human intuition and prior experience—therefore sticking to known and understood mechanisms rather than exploring entirely new possibilities—and by mimicking nature.[4] Such an approach works reasonably well for some specific cases, but cannot guarantee high

efficiency in general, and may not be ideal for applications in industrial setting. An alternative strategy for the design process of mechanical metamaterials is the "automated design,"[1] as it uses robust computational methods to obtain a rich variety of complex structures optimized over a given feature, difficult to realize with heuristic-driven approaches. Topological optimization (TO) is one of the most known methods for numerically designing periodic lattice structures, which consists of maximizing a weighted objective function formulated to achieve optimization of the architecture under predetermined constraints and loads within a continuum finite element approach.[5] TO typically focuses on optimizing the overall mechanical response to external stimuli, such as the design of metamaterials with graded Young's modulus,[5] thus dealing with static structures instead of functional metamaterial actuators.

Recently, we proposed a fully automated strategy to create metamaterial actuators, able to provide the desired response to any type of mechanical functional requirement.[6] Our method couples discrete element simulations with optimization algorithms for the generation of two-dimensional (2D) functional mechanical metamaterials. In this paper, we propose a generalization of the algorithm to three-dimensional (3D) structures. This allows us to treat more complex input–output scenarios and design a wider variety of functional metamaterials. In particular, we test the algorithm to the case of tension–torsion mechanism, which represents the key property of the so-called *chiral* mechanical metamaterials.

Chirality is the widespread intrinsic characteristic of systems that are distinguished from their mirror image, which is typical of many biological structures, such as organic molecules, DNA, proteins, and even large scale structures, such as plants or shells.[7–9] Artificially designed chiral structures, inspired by nature, such as screws and propellers, are widely used for industrial applications.[10] Chirality might be present in the structure itself, or could only occur under external stimuli, as an electric field or mechanical compression/tension. The ability to twist under compression/tension is normally not present in ordinary materials whose elastic behavior is described by Cauchy continuum mechanics. On the other hand, mechanical metamaterials with artificially designed composite architectures may activate torsional degrees of freedom by breaking the cylindrical symmetry of the sample,[11] implementing an effective chiral mechanism.

While the theory of chiral mechanical materials was developed a decade ago,[12] the practical realization of chiral metamaterials was achieved only later,[13–17] thanks to the advances in additive manufacturing techniques. For example, Frenzel *et al.*[14] proposed a microstructured 3D mechanical metamaterial with a cubic unit cell and a tetrachiral lattice on each face, showing torsion up to 2 degrees of rotation per percentage axial compression strain. Other types of chiral metamaterials were designed by extending a 2D lattice to 3D by rolling it over a cylindrical tube[18] or a cylindrical shell, taking inspiration from plant architectures.[19] Chiral metamaterials were also obtained using microstructures of auxetic metamaterials designed by topology optimization (TO).[20] Furthermore, TO of tubes or beams with twisting deformations upon axial strains was also achieved using TO for bi-material chiral auxetic microstructures.[20] Finally, chiral mechanical metamaterials were designed using an automated generative algorithm, which enabled excellent twist-compression efficiency.[21] Probably, the simplest chiral metamaterials were obtained using a cubic frame endowed with diagonal beams on its faces.[22,23]

Here, we apply our discrete element based algorithm to automatically design efficient chiral metamaterial architectures, starting from a three-dimensional elastic lattice. Our main motivation is to check whether such machine-generated metamaterials can outperform previous human-designed structures.[13–17,22] As shown below, very different solutions can be obtained depending on the initial lattice geometry and on the choice of the efficiency function that governs the optimization algorithm.

This paper is organized as follows: in Sec. II, we describe the algorithm, which is then simulated in Sec. III. In Sec. IV, we validate the automatically designed structure experimentally using 3D printing, and in Sec. V, we conclude.

II. ALGORITHM

A. Initial configuration

As the initial configuration for our optimization search, we consider a face centered cubic (FCC) lattice with coordinates $\{\mathbf{R}\} = (\mathbf{r}_1, \mathbf{r}_2, \ldots, \mathbf{r}_N)$. Using this lattice structure is useful since it allows us to compare with some available human-designed chiral unit cells. The initial configuration is mechanically stable and is composed of N_b beams of length r_0 connecting N nodes. The position of the ith node is $\mathbf{r}_i = (x_i, y_i, z_i)$, and the distance between the two nodes is $r_{ij} = |\mathbf{r}_j - \mathbf{r}_i|$.

We select two groups of nodes as input and output regions. For each node i in those groups, we define a normalized vector identifying the desired deformation direction, $\mathbf{t}_i^{\text{inp}}$ and/or $\mathbf{t}_i^{\text{out}}$. To design a chiral structure, the displacements $\mathbf{t}_i^{\text{inp}}$ of all the input nodes are chosen to be parallel to the z axis, pointing toward the compressive direction, while the output nodes coincide with the input ones and are free to move in the xy plane so as to allow rotational movement. The magnitude of displacement for the input nodes, δ, is quantified by the axial strain $s = \frac{\delta L}{L} = 0.01$, where L is the rest length of the structure along the z direction. To sustain the compression, the bottom layer is kept fixed.

B. Twist-compression efficiency

The response of the metamaterial is monitored through its twist-compression efficiency η, which quantifies how well the structure is able to perform the desired task. The aim is to maximize the torsion of the metamaterial in the xy plane perpendicular to the vertical axial compression along z. Compression corresponds to a downward displacement δ of the upper input nodes, the displacement being identical for all input nodes by construction. At each step of the optimization, the angular displacement of each output node j is evaluated by calculating the angle of rotation with respect to its rest position,

$$\delta\theta_j = \arctan\frac{y_j}{x_j} - \arctan\frac{y_{0j}}{x_{0j}}, \tag{1}$$

where the subscript 0 indicates the initial rest coordinates. Since we are dealing only with relatively small displacements, we can safely assume $|\delta\theta_j| < \pi$. To implement this assumption, we map all the possible values of $\delta\theta_j$ in the interval $[-\pi, \pi]$ via the minimum-image convention.

The overall efficiency is obtained by averaging $\delta\theta_j$ over all the output nodes and by dividing by the vertical compressive strain,

$$\eta = \frac{1}{m}\sum_{j=1}^{m}\left(\delta\theta_j - 2\pi\left\lfloor\frac{1}{2} + \frac{\delta\theta_j}{2\pi}\right\rfloor\right)\frac{1}{s}, \tag{2}$$

where m is the number of output nodes and $\lfloor x \rfloor$ is the floor function, yielding as output the greatest integer less than or equal to x. As shown later, the angular displacement is not proportional to the applied strain, showing nonlinearity already at few percentage strains. For small enough strains, this relationship can be fairly well approximated to be linear so that η is strain independent. In this limit, one could compute the efficiency from the Hessian, although the method is not necessarily faster for complex interaction potentials like the ones used here and for a large number of nodes.

C. Optimization

Once a suitable efficiency function is chosen, we maximize it by minimizing the cost function $\Delta = -\eta$. Since η is dependent on strain, in the minimization process, we set $s = 0.1$. The minimization protocol is based on the Monte Carlo (MC) method combined with an energy-minimization algorithm:[1] at each iteration step, from the present configuration with $\Delta = \Delta^0$, a trial configuration is obtained by removing or re-adding a randomly selected beam. Beams connecting the input or output nodes are discarded from pruning as well as those connecting nodes constrained against motion (i.e., frozen nodes). Then, the input nodes are displaced in the $\mathbf{t}^{\text{inp}}$ direction, and a Fast Inertial Relaxation Engine (FIRE) optimization[24] is performed. By the displacement of the output nodes, the efficiency function is evaluated alongside the associated Δ^{trial}. If $\Delta^{trial} < \Delta^0$, the removal/re-adding of the beam is accepted; otherwise, it is accepted with a probability $P = \exp[-(\Delta^{trial} - \Delta^0)/T]$, where T is a parameter acting as temperature in the MC dynamics. Note that in this work, we are not concerned with detailed balance, which is only relevant to ensure that the MC converges to thermodynamic equilibrium.

It is important to remark that for a system with N_b beams, the configuration space displays $\sim 2^{N_b}$ possible structures making brute force exact optimization particularly challenging even for relatively small samples. To improve the performance of the MC search, we use simulated annealing,[25] which is known to be well suited for problems with a complex landscape like the present one. At the beginning of each run, we perform 100 (accepted) MC steps of annealing with T linearly decreasing from $T = 0.06$ (which is the threshold to consistently get $P \simeq 1$) to $T = 0$, and we subsequently let the algorithm evolve at the latter temperature. The whole procedure has been repeated in several runs using different seeds for the random number generator (see supplementary material Fig. 1).

We also use symmetry-based arguments to help the search of suitable structures. Without imposing constraints on the rotational symmetry of the structure, one could easily obtain configurations in which the resulting force is not purely torsional, producing lateral bending or misalignments during motion. To circumvent these drawbacks, we have therefore introduced a C_4 rotational symmetry constraint around the z axis. This means that each beam belongs to an equivalence class determined by discrete rotations of 90°. When the algorithm decides to delete (or add) a beam, all four beams from the same equivalence class will be affected. This rule not only ensures symmetrical configurations but also that at least four beams connecting the topmost and bottommost layers will be present. A secondary but computationally advantageous consequence of this choice is that the effective configuration space in which the algorithm searches for the optimal configuration is reduced by a quarter.

D. Discrete element model

To obtain a fast and reliable estimation of the efficiency of a given structure, we employ a simplified discrete element model (DEM) of the lattice, whose total energy can be expressed as

$$E = \sum_i\sum_{j>i}\phi_2(\mathbf{r}_{ij}) + \sum_i\sum_{j>i}\sum_{k\neq j}\phi_3(\mathbf{r}_{ij},\mathbf{r}_{ik},\theta_{ijk}) + \\ + \sum_{i,j,k,l}\phi_4(\mathbf{r}_{ij},\mathbf{r}_{jk},\mathbf{r}_{kl},\varphi_{ijkl}), \tag{3}$$

where the two-body term is a spring potential with the rest length r_0 [Fig. 1(a)],

$$\phi_2(\mathbf{r}_{ij}) = k_b(\mathbf{r}_{ij} - \mathbf{r}_0)^2, \tag{4}$$

while the three-body term introduces angular springs among the nearest neighbor beams connected to the same node [see Fig. 1(b)],

$$\phi_3(\mathbf{r}_{ij},\mathbf{r}_{ik},\theta_{ijk}) = k_a\left[\theta_{ijk} - \theta^0_{ijk}\right]^2, \tag{5}$$

where θ_{ijk} is the angle formed by the beams $\overline{ij}$ and $\overline{ik}$, and θ^0_{ijk} is the rest angle in the FCC lattice. The four-body term introduces angular springs between the dihedral angles defined by four consecutive nonaligned nodes [see Fig. 1(c)],

$$\phi_4(\mathbf{r}_{ij},\mathbf{r}_{jk},\mathbf{r}_{kl},\varphi_{ijkl}) = k_d\left[\varphi_{ijkl} - \varphi^0_{ijkl}\right]^2, \tag{6}$$

where φ_{ijkl} is the angle formed by the two planes of the dihedral: the first plane is determined by the beams $\overline{ij}$ and $\overline{jk}$, and the second plane is formed by the beams $\overline{jk}$ and $\overline{kl}$.

The minimization of E in the presence of frozen nodes (typically at the base of the structure) and of displaced input nodes allows us to predict the response of the trial structure with a good compromise between speed and reliability.

E. Finite element method

To parameterize our DEM potential and to validate the final efficiency of the DEM generated structures, we use a finite element method (FEM) as implemented by COMSOL Multiphysics and COMSOL with MATLAB through its structural mechanics module.[26] All studies assume a linear elastic material with Young's modulus $Y = 80$ MPa and Poisson's ratio $\nu = 0.45$, estimated experimentally for the bulk samples of interest. Results are obtained using Euler–Bernoulli beam elements and the in-built stationary studies calculation (a quasi-static solver). The FEM is based on a mesh representation of the object so that the continuum boundary value problem is transformed into a system of algebraic equations. The method is very accurate in the elastic regime but works on the timescale of several seconds for our reference system (and rapidly increasing with the system size), and it is thus not suitable for the trial-error MC search of efficient structures. Rather, the FEM has

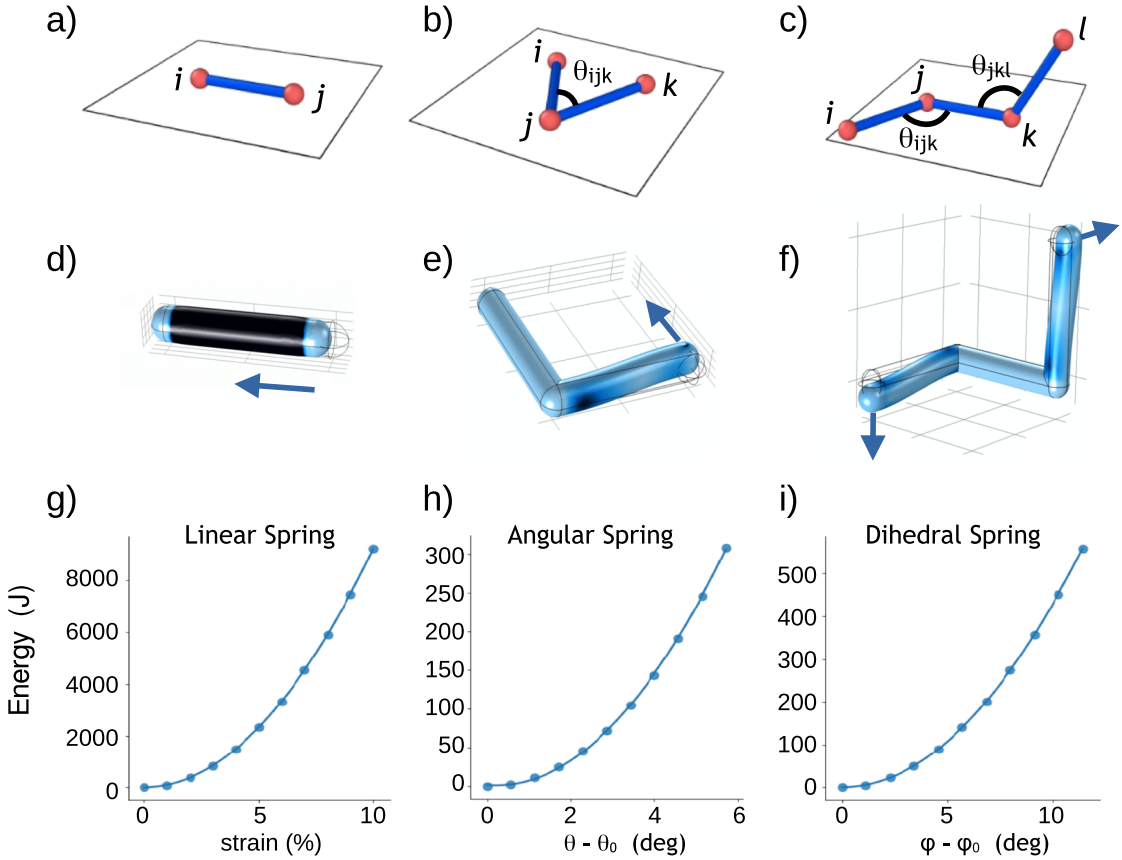

FIG. 1. Parameterization of the DEM. The three elementary discrete elements used in the DEM correspond to three interaction terms in the energy. We report the discrete elements corresponding to (a) a linear spring describing bond stretching/compression, (b) an angular spring describing bending, and (c) a dihedral term describing torsion. The corresponding finite element method (FEM) simulations performed with COMSOL are reported in panels (d)–(f). Here, the color code represents the value of the von Mises stress. Panels (g)–(i) report the energy terms corresponding to each of the three terms. Parameters have been adapted so that the DEM and FEM results agree.

been employed before 3D printing as a final validation of the efficiency of the selected structures generated through the more simplified and fast DEM methods described above.[6] The DEM spring constants are parameterized by simulating with FEM the longitudinal (k_b) angular (k_a) and torsional (k_d) displacement of the 3D beams, in order to extract the energy contributions corresponding to the three DEM terms of Eq. (3) [see Figs. 1(d)–1(f)]. By a parabolic fitting of the resulting energy curves at low strain [Figs. 1(g)–1(i)], we could obtain the corresponding spring constants. This procedure, performed with beams of diameter $d = 3.5$ mm and length $l = 20\sqrt{2}$ mm, resulted in the following parameters: $k_b = 5.54 \times 10^4$ J/m^2, $k_a = 0.48$ J/rad^2, and $k_d = 0.096$ J/rad^2. Noting that $l \cdot k_b/k_a = 92.43$ and $l \cdot k_b/k_d = 461.2$, we have used the following parameters in reduced units: $k_b = 10$, $k_a = 10/92.43 = 0.108$, $k_d = 10/461.2 = 0.022$, and $r_0 = 1$.

III. NUMERICAL SOLUTIONS

A. Optimal structures

To test the performance of our design algorithm, we perform a series of MC simulations and monitor the torsion/compression efficiency as a function of simulation time. As shown in Fig. 2, the algorithm is able to find solutions that reach high efficiency, outperforming the efficiency of the human-designed structures reported in Refs. 14 and 22.

We consider two different strategies to find efficient structures: in the *surface* realization, we confine all the beams on the surface of the cube, leaving the interior devoid of bonds, while in the *bulk* realization, we consider all the beams in the lattice. In Fig. 3, we report optimal structures obtained by the algorithm for the surface [Fig. 3(b)] and bulk realizations [Fig. 3(c)] compared for reference with the simple diagonal structure proposed in Ref. 22 (see supplementary material, videos S1–S3). Note that some links in the machine-designed structure carry no load. These links could safely be removed if so desired, since they do not affect the efficiency. We then report in Fig. 3(d) the torsional angle as a function of the compressive strain for the three reported structures. The results are obtained with DEM and FEM and show a good agreement between the two methods, with deviations at large strains. We notice also that there is a nonlinear relation between torsion angle and compressive strain. This implies that the efficiency is a strain-dependent quantity.

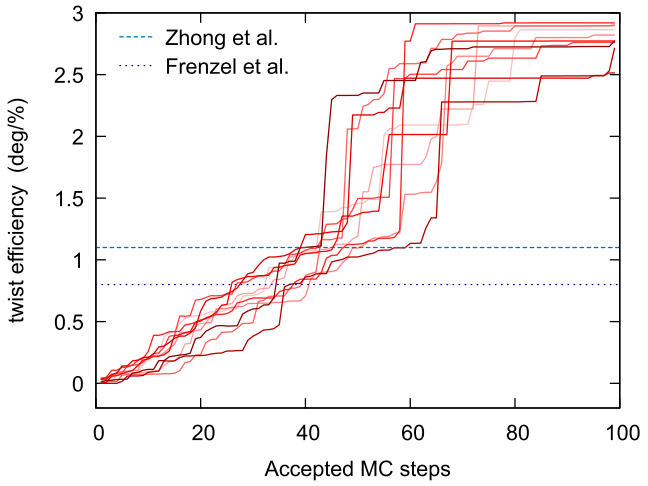

FIG. 2. Efficiency evolution during optimization. Plot of instantaneous η during different realizations of the MC algorithm. Each curve is obtained with a different initial random seed. Only the efficiency corresponding to accepted MC steps is reported. Dashed and dotted lines mark the efficiency of the human-designed structures from the work of Zhong *et al.*[22] and Frenzel *et al.*,[14] respectively. The efficiency has been recomputed with our code to ensure uniformity in terms of parameter values and aspect ratio.

B. Performance of the algorithm

Following the analysis of Ref. 6 for the 2D algorithm, we study the scaling of the algorithm from an empirical perspective. To this end, we prepare four lattices of increasing size from $N_b = 96$ to $N_b = 480$ bonds. We then run our algorithm for a total of $10 \cdot N_b$ accepted MC steps, decreasing the temperature from 0.06 to 0, followed by $2 \cdot N_b$ MC steps at zero temperature. We generate ten different structures for each lattice size, totaling 40 structures. For each resulting structure, we measure its efficiency η [Fig. 4(a)] and the total execution time τ [Fig. 4(b)]. As for the 2D case, the efficiency of the optimized configurations increases with N_b.

A scaling exponent α is obtained by fitting a liner regression model between $\log \tau$ and $\log N_b$. We obtain an estimate of $\hat{\alpha} = 2.36$. This value is slightly smaller than the one reported in Ref. 6 for the 2D system, likely due to the fact that we have improved the performance of the energy relaxation routine.

IV. EXPERIMENTAL VALIDATION

For the experimental validation of the model, we produced a sample corresponding to the most efficient structure [reported in Fig. 3(c)] with a Multi Jet Fusion 3D printer (HP Jet Fusion 4200) using Ultrasint TPU 90A-01, a thermoplastic polyurethane. The 3D printed sample is reported in Fig. 5(a).

Mechanical tests were performed on the 3D printed sample by means of a multiaxial, electro-dynamic testing machine (Instron ElectroPuls E3000). Such a machine is able to guarantee an accuracy of 0.15 N and 0.001 25 Nm for axial force and torsional moment, respectively. Mechanical tests were performed at room temperature by securing samples to compressive plates by means of adhesive tape, in order to avoid undesired slipping during testing. Thereafter, compression was imposed by controlling the descent of upper

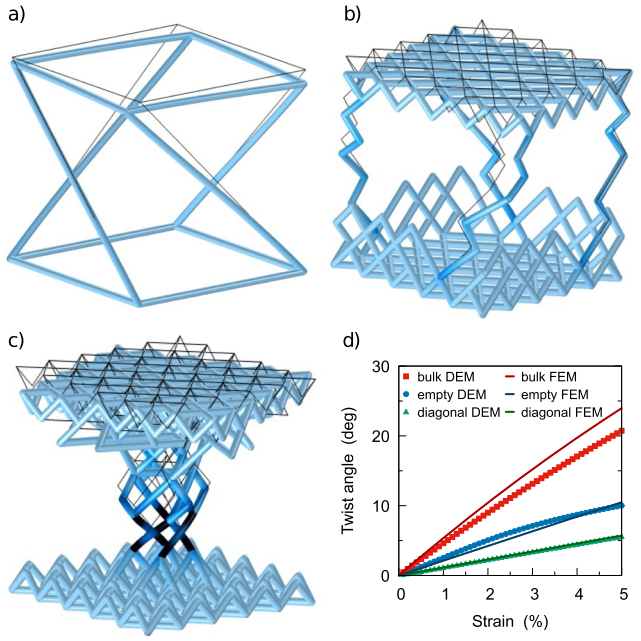

FIG. 3. Reference optimal structures. Perspective view of (a) the diagonal structure proposed in Ref. 22 and of automatically designed structures starting from (b) the empty lattice and (c) the FCC lattice. Structures show a twisting in response to a vertical compression—the resting configuration is shown in black thin lines. A darker color of the beams corresponds to a larger local stress. (d) For the structures in panels (a)–(c), we report the torsional angle as a function of the applied vertical strain evaluated with the DEM and FEM.

compression plate to −10 mm while keeping the rotary momentum equal to 0 Nm: as a consequence, the structure could rotate freely about its axis while being compressed. This allowed us to register the obtained rotary displacement of the structure as a function of the applied linear displacement, therefore confirming the functionality of the designed structure. The torsional angle as a function of strain follows the trend predicted numerically (see supplementary material, video S4). In particular, we observe a nonlinear increase in the torsional angle with the compressive strain as shown in Fig. 5(b) for different strain rates. The intermittent steps observed in the curve are due to the lags in the response of the machine, but the general trend expected from the simulation is followed by experiments. In

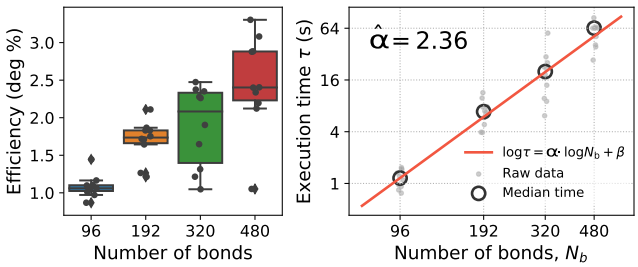

FIG. 4. Scaling of the algorithm. (a) Boxplot of the efficiency as a function of the system size evaluated over ten runs for each size and (b) increase in the execution time as a function of the system size for the same set of panel (a).

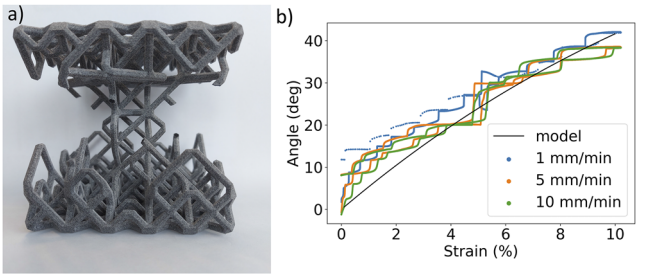

FIG. 5. Experimental results. (a) The 3D printed structure corresponding to Fig. 3(c). (b) The deformation curves reporting the effective torsion angle as a function of the strain for three different deformation rates. Both loading and unloading curves are reported. The black line is the result of FEM simulations for the same structure.

particular, the measured twist-compression efficiency is comparable with the predictions.

V. CONCLUSION

In this paper, we have presented an algorithm to generate automatically three-dimensional mechanical metamaterial actuators with predefined functions. The algorithm is based on a combination of DEM and MC optimization following the steps of a previously introduced two-dimensional algorithm.[6] The extension to three dimensions brings additional technical complexity related to the appearance of torsional interactions not present in two dimensions. To deal with this issue, we introduce a dihedral term in the DEM, in addition to linear and angular springs already present in two dimensions. To find the best effective parameters of the DEM, we compare the elastic energy of elementary configurations computed with the DEM and FEM, as implemented in COMSOL.[26] In this way, the DEM provides a reasonable approximation to the elastic deformations of a structure under load. While the DEM provides only an approximate solution to the elastic behavior, it allows for a rapid search in the configuration space. The resulting structures found using the DEM can then be tested with the FEM to assess more precisely their efficiency. This strategy avoids lengthy iteration of more computationally heavy FEM calculations, employed, for instance, in TO schemes.

We applied our strategy to the design of chiral mechanical metamaterials that convert vertical compression into rotation. In this case, the efficiency is defined as the rotation angle per unit strain. Several examples of human-designed chiral mechanical metamaterials have recently appeared in the literature.[13–17,22] The structures designed by our algorithm, however, display higher efficiency with respect to the human-designed one. While we validated the algorithm for this particular example, the strategy is more general and can readily be applied to a wide variety of cases as for the two-dimensional case explored in Ref. 6.

We chose to optimize the metamaterial structure only in terms of the twist/compression efficiency. As a result of this, the structure we obtain sustains larger stresses than previously designed but less efficient structures. It is possible, in principle, to modify the algorithm to take into account a stress-dependent efficiency as already discussed in Ref. 6.

Several classes of metamaterials are constructed by repeating an individual cell over a periodic pattern. It is thus interesting to discuss how the efficiency would change if the actuating cell we designed is repeated into a periodic pattern. As discussed in Ref. 14, if we simply pile up more actuator units, we would increase the efficiency proportionally to their number. The other possibility is to laterally repeat the unit cell, for example, in a $M \times M$ grid (e.g., 3×3, 4×4, and so on; see Figs. 2 and 3 of Ref. 14). In such a case, we expect that the total efficiency would decrease for higher M, approaching zero efficiency in the limit $M \to \infty$ in analogy with the results of Ref. 14. This is a general property of twist/compression chiral metamaterials that can only be studied with open boundary conditions, in contrast with the periodic boundary conditions employed for other types of metamaterials. For example, periodic boundary conditions were used in Ref. 20 to design by TO a two-dimensional cell that would twist under *biaxial* compression. The same cell was then used in a sheet rolled into a cylinder with open boundaries that displayed twist under *uniaxial* compression. The resulting efficiency ($\eta \simeq 1.5\ ^\circ/\%$) was, however, moderately small.

SUPPLEMENTARY MATERIAL

The supplementary material includes four movies describing finite element simulations for the compression of the three structures reported in Fig. 3 and a representative movie of the experiment described in Fig. 5.

ACKNOWLEDGMENTS

This work was supported by the SEED4IP-METAMECH proof of concept project funded by the Ministry of Economic Development. The authors S.B., R.G., and S.Z. declare the following competing interests: the University of Milan has filed a patent application related to this work. Inventors: S. Bonfanti, R. Guerra, and S. Zapperi. Patent status: pending. Date of application: 19/11/2019. Application No. 102019000021618. The patent concerns a design method for mechanical actuators.

AUTHOR DECLARATIONS

Conflict of Interest

The authors have no conflicts to disclose.

DATA AVAILABILITY

The data that support the findings of this study are available from the corresponding author upon reasonable request.

REFERENCES

[1] S. Bonfanti, R. Guerra, M. Zaiser, and S. Zapperi, "Digital strategies for structured and architected materials design," APL Mater. **9**(2), 020904 (2021).
[2] D. Rayneau-Kirkhope, S. Bonfanti, and S. Zapperi, "Density scaling in the mechanics of a disordered mechanical meta-material," Appl. Phys. Lett. **114**(11), 111902 (2019).
[3] A. Ion, J. Frohnhofen, L. Wall, R. Kovacs, M. Alistar, J. Lindsay, P. Lopes, H.-T. Chen, and P. Baudisch, "Metamaterial mechanisms," in *Proceedings of the 29th Annual Symposium on User Interface Software and Technology* (ACM, 2016), pp. 529–539.
[4] C. A. M. La Porta, M. C. Lionetti, S. Bonfanti, S. Milan, C. Ferrario, D. Rayneau-Kirkhope, M. Beretta, M. Hanifpour, U. Fascio, M. Ascagni *et al.*, "Metamaterial

architecture from a self-shaping carnivorous plant," Proc. Natl. Acad. Sci. U. S. A. **116**(38), 18777–18782 (2019).
[5]E. C. Joseph, S. Zhou, Y. Chen, and Q. Li, "On design of multi-functional microstructural materials," J. Mater. Sci. **48**(1), 51–66 (2013).
[6]S. Bonfanti, R. Guerra, F. Font-Clos, D. Rayneau-Kirkhope, and S. Zapperi, "Automatic design of mechanical metamaterial actuators," Nat. Commun. **11**(1), 4162 (2020).
[7]B. Lotz, A. Gonthier-Vassal, A. Brack, and J. Magoshi, "Twisted single crystals of *Bombyx mori* silk fibroin and related model polypeptides with β structure: A correlation with the twist of the β sheets in globular proteins," J. Mol. Biol. **156**(2), 345–357 (1982).
[8]R. Paniagua, M. Royuela, R. M. Garcia-Anchuelo, and B. Fraile, "Ultrastructure of invertebrate muscle cell types," Histol. Histopathol. **11**, 181 (1996).
[9]Y. Forterre and J. Dumais, "Generating helices in nature," Science **333**(6050), 1715–1716 (2011).
[10]W. Chen, D. Ruan, and X. Huang, "Optimization for twist chirality of structural materials induced by axial strain," Mater. Today Commun. **15**, 175–184 (2018).
[11]I. Fernandez-Corbaton, C. Rockstuhl, P. Ziemke, P. Gumbsch, A. Albiez, R. Schwaiger, T. Frenzel, M. Kadic, and M. Wegener, "New twists of 3D chiral metamaterials," Adv. Mater. **31**(26), 1807742 (2019).
[12]A. C. Eringen, *Microcontinuum Field Theories: I. Foundations and Solids* (Springer Science & Business Media, 2012).
[13]C. S. Ha, M. E. Plesha, and R. S. Lakes, "Chiral three-dimensional isotropic lattices with negative Poisson's ratio," Phys. Status Solidi B **253**(7), 1243–1251 (2016).
[14]T. Frenzel, M. Kadic, and M. Wegener, "Three-dimensional mechanical metamaterials with a twist," Science **358**(6366), 1072–1074 (2017).
[15]J. I. Lipton, R. MacCurdy, Z. Manchester, L. Chin, D. Cellucci, and D. Rus, "Handedness in shearing auxetics creates rigid and compliant structures," Science **360**(6389), 632–635 (2018).
[16]S. Duan, W. Wen, and D. Fang, "A predictive micropolar continuum model for a novel three-dimensional chiral lattice with size effect and tension-twist coupling behavior," J. Mech. Phys. Solids **121**, 23–46 (2018).
[17]M. Fu, F. Liu, and L. Hu, "A novel category of 3D chiral material with negative Poisson's ratio," Compos. Sci. Technol. **160**, 111–118 (2018).
[18]W. Wu, L. Geng, Y. Niu, D. Qi, X. Cui, and D. Fang, "Compression twist deformation of novel tetrachiral architected cylindrical tube inspired by towel gourd tendrils," Extreme Mech. Lett. **20**, 104–111 (2018).
[19]C. Ma, H. Lei, J. Hua, Y. Bai, J. Liang, and D. Fang, "Experimental and simulation investigation of the reversible bi-directional twisting response of tetra-chiral cylindrical shells," Compos. Struct. **203**, 142–152 (2018).
[20]H. Zhang, Y. Luo, and Z. Kang, "Bi-material microstructural design of chiral auxetic metamaterials using topology optimization," Compos. Struct. **195**, 232–248 (2018).
[21]D. Goswami, Y. Zhang, S. Liu, O. A. Abdalla, P. D. Zavattieri, and R. V. Martinez, "Mechanical metamaterials with programmable compression-twist coupling," Smart Mater. Struct. **30**(1), 015005 (2020).
[22]R. Zhong, M. Fu, X. Chen, B. Zheng, and L. Hu, "A novel three-dimensional mechanical metamaterial with compression-torsion properties," Compos. Struct. **226**, 111232 (2019).
[23]P. Ziemke, T. Frenzel, M. Wegener, and P. Gumbsch, "Tailoring the characteristic length scale of 3D chiral mechanical metamaterials," Extreme Mech. Lett. **32**, 100553 (2019).
[24]E. Bitzek, P. Koskinen, F. Gähler, M. Moseler, and P. Gumbsch, "Structural relaxation made simple," Phys. Rev. Lett. **97**(17), 170201 (2006).
[25]S. Kirkpatrick, C. D. Gelatt, and M. P. Vecchi, "Optimization by simulated annealing," Science **220**(4598), 671–680 (1983).
[26]Comsol Multiphysics (version 4.3a), https://www.comsol.com/comsol-multiphysics, 2012.